Article

NMR Magnetic Shielding in Transition Metal Compounds Containing Cadmium, Platinum, and Mercury

Andy D. Zapata-Escobar [1,2], Alejandro F. Maldonado [2], Jose L. Mendoza-Cortes [3] and Gustavo A. Aucar [1,2,*]

1   Natural and Exact Science Faculty, National Northeastern University of Argentina, Avda. Libertad 5460, Corrientes W3404AAS, Argentina; danianescobar@gmail.com
2   Institute of Modeling and Innovative Technology (CONICET-UNNE), Corrientes W3404AAS, Argentina; aleomlagain@gmail.com
3   Department of Chemical Engineering & Materials Science, Michigan State University, East Lansing, MI 48824, USA; jmendoza@msu.edu
*   Correspondence: gaaucar@conicet.gov.ar

Abstract: In this article, we delve into the intricate behavior of electronic mechanisms underlying NMR magnetic shieldings σ in molecules containing heavy atoms, such as cadmium, platinum, and mercury. Specifically, we explore PtX_n^{-2} (X = F, Cl, Br, I; n = 4, 6) and $XCl_2Te_2Y_2H_6$ (X = Cd, Hg; Y = N, P) molecular systems. It is known that the leading electronic mechanisms responsible for the relativistic effects on σ are well characterized by the linear response with elimination of small components model (LRESC). In this study, we present the results obtained from the innovative LRESC-Loc model, which offers the same outcomes as the LRESC model but employs localized molecular orbitals (LMOs) instead of canonical MOs. These LMOs provide a chemist's representation of atomic core, lone pairs, and bonds. The whole set of electronic mechanisms responsible of the relativistic effects can be expressed in terms of both non-ligand-dependent and ligand-dependent contributions. We elucidate the electronic origins of trends and behaviors exhibited by these diverse mechanisms in the aforementioned molecular systems. In PtX_4^{-2} molecules, the predominant relativistic mechanism is the well-established one-body spin–orbit ($\sigma^{SO(1)}$) mechanism, while the paramagnetic mass–velocity (σ^{Mv}) and Darwin (σ^{Dw}) contributing mechanisms also demand consideration. However, in PtX_6^{-2} molecules, the $\sigma^{(Mv/Dw)}$ contribution surpasses that of the $SO(1)$ mechanism, thus influencing the overall ligand-dependent contributions. As for complexes containing Cd and Hg, the ligand-dependent contributions exhibit similar magnitudes when nitrogen is substituted with phosphorus. The only discrepancy arises from the $\sigma^{SO(1)}$ contribution, which changes sign between the two molecules due to the contribution of bond orbitals between the metal and tellurium atoms.

Keywords: transition metals; LRESC-Loc; magnetic shielding; relativistic effects

1. Introduction

Transition metal chemistry represents a field of study characterized by a rich historical background and ongoing advancements. A profound comprehension of organometallic complex properties and the underlying reaction mechanisms has paved the way for the development of practical methodologies widely employed in synthetic chemistry. Moreover, transition metals find utility as Lewis acids, heterogeneous catalysts, and polymerization catalysts, among other roles [1].

While the application of methods of the density functional theory (DFT) to calculate the spectroscopic parameters of the nuclear magnetic resonance (NMR) of transition metals has been previously reviewed [2,3], discussions pertaining to those calculations on heavier transition metal complexes are found within reviews that focus specifically on relativistic methodologies. This emphasis stems from the significant influence of relativistic effects on the spectroscopic parameters associated with such complexes [4–7].

In this work, we wanted to explore the NMR spectroscopic parameters of some particular transition-metal-containing compounds. They contain Cd, Hg and Pt. In a seminal work, Gilbert and Ziegler achieved remarkable accuracy in predicting ^{195}Pt chemical shifts for a series of Pt(II) complexes by meticulously unraveling the contributing parameters responsible for the shielding of platinum nuclei [8]. Their study underscored the dominant influence of paramagnetic and spin–orbit contributions on the overall shielding. Building upon this results, numerous theoretical and experimental investigations have explored the chemical shifts of platinum halides in square–planar (D_{4h}) and octahedral (O_h) complexes [8–13], with some studies employing localized molecular orbitals (LMOs) as an analytical framework [14,15]. Concerning the other two transition metals, i.e., Cd and Hg, we want to point to a computational NMR study conducted on recently synthesized complexes encompassing cadmium, mercury, tellurium, selenium, and phosphorus [16]. These complexes, known as MRE complexes, were identified as promising qubit molecules for NMR quantum information processing (QIP). Employing spin–orbit zeroth-order regular approximation (ZORA) and four-component (4C) relativistic methods, the researchers presented a comprehensive computational design strategy for screening molecules suitable for diverse and heteronuclear qubits in NMR-QIP implementations. Their investigation encompassed the influence of different conformers, basis sets, functionals, as well as methods to account for relativistic and solvent effects.

It is known that the nuclear magnetic shielding of the NMR spectroscopy, denoted as σ, is a highly sensitive quantity influenced by the electronic environment. Consequently, it serves as a valuable descriptor of the electronic behavior in the vicinity of the nucleus under investigation, offering insights into the nature of the involved bonding interactions [17]. When heavy atoms (HAs) are present in a molecule, they introduce relativistic effects that impact the neighboring atoms as well as themselves. There are three well-established types of relativistic effects described in the literature: (i) the heavy atom on light atom (HALA) effect [18], the heavy-atom effect on the heavy atom itself [19] and the heavy-atom effect on vicinal-heavy-atom (HAVHA) effect [20,21]. The HALA effect is the most studied, being the basic rule of propagation of the SO effect on a molecule since more than twenty years ago [22]. It can show some characteristics of the HA-LA bond and the structure of the heavy atom [7]. The HAHA effect is less studied because its inclusion gives more accurate absolute values of σ but it does not contribute much to the chemical shift. On the other hand, the HAVHA effect is currently being more studied because its description requires considering other mechanisms different from the SO one. Then the characteristics of the bonds between two heavy atoms are better described through including some more ligand-dependent mechanisms.

Several years ago, Autschbach introduced the London orbitals and the interface with natural bond orbitals (NBOs) in the calculation of the shielding tensor that include scalar relativistic corrections [15]. In a similar vein, Marek and colleagues investigated various systems encompassing different heavy atoms across the periodic table, studying trends in the HALA effect. They called it SO-HALA to emphasize that HALA effects mainly arise from spin–orbit couplings. Their studies involved the inclusion of those corrections through third-order perturbation theory, revealing the increase in the HALA effect when lone pair electrons are involved [7,17,23].

Another model that has been developed over the past two decades with the objective of accurately reproducing and analyzing the electronic origins of NMR spectroscopic parameters is the linear response with elimination of small component model (LRESC) [24–26]. This model enables a comprehensive understanding of the electronic mechanisms responsible for relativistic effects. To this end, the LRESC-Loc model is a scheme that was recently introduced [27] to facilitate the analysis of various types of localization procedures (such as Pypek–Mezey [28] or natural bond orbitals (NBOs) [29]) for obtaining localized molecular orbitals (LMOs) and providing a chemical representation of atomic core, lone pairs, and chemical bonds in elucidating well-known relativistic effects.

In this work, we delve into the nuclear magnetic shielding properties of cadmium, platinum, and mercury nuclei within PtX_n^{-2} (X = F, Cl, Br, I; n = 4, 6) and $Cl_2XTe_2Y_2H_6$ (X = Cd, Hg; Y = P, N) molecular systems, employing both the LRESC-Loc and the four-component (4C) relativistic methods. The primary purpose of this study is related to understanding the origin and behavior of relativistic corrections expressed in terms of LMOs. Specifically, we investigate the influence of the chemical environment on the shielding of the transition metals under investigation through the mechanisms known as ligand dependence and considering both the HAHA and the HAVHA effects. We shall show how important the electronic mechanisms involved are and how much each LMO contributes to such mechanisms. It will be shown that the SO is not the main mechanism contributing to the shielding of some of the transition metals analyzed. This is one of the results that appears when the HAVHA effects are considered.

2. Theoretical Framework

The LRESC model is a robust methodology rooted in second-order Rayleigh–Schrödinger perturbation theory (RSPT), which enables the transformation of four-component (4C) wave functions to two-component (2C) wave functions for describing magnetic and electric properties [24,26,30]. Within the LRESC model, the final expressions encompass several electronic mechanisms incorporating relativistic corrections at different levels of the selected parameter (1/c) (c being the speed of light in vacuum).

Specifically, in the studies of NMR nuclear magnetic shieldings, the LRESC approach facilitates the calculation of relativistic corrections for both paramagnetic and diamagnetic nonrelativistic (NR) components. This is accomplished through a rewriting of the 4C expression while adhering to the kinetic balance condition and Pauli normalization, and incorporating relativistic corrections into the Pauli wave function. For further in-depth information, additional references can be consulted [24–26].

The paramagnetic component of the nuclear magnetic shielding involves several relativistic corrections which are expressed up to the order c^{-2} as follows:

$$\sigma^{OZ-K} = \langle\langle H^{PSO}; H^{OZ-K}\rangle\rangle \tag{1}$$

$$\sigma^{PSO-K} = \langle\langle H^{OZ}; H^{PSO-K}\rangle\rangle \tag{2}$$

$$\sigma^{(FC/SD)-K} = \langle\langle H^{FC/SD}; H^{SZ-K}\rangle\rangle \tag{3}$$

$$\sigma^{(FC/SD)-BSO} = \langle\langle H^{FC/SD}; H^{BSO}\rangle\rangle \tag{4}$$

$$\sigma^{SO(1)} = \langle\langle H^{PSO}; H^{FC+SD}, H^{SO(1)}\rangle\rangle \tag{5}$$

$$\sigma_p^{(Mv/Dw)} = \langle\langle H^{PSO}; H^{OZ}, H^{Mv/Dw}\rangle\rangle \tag{6}$$

In these expressions, H^{PSO} and H^{OZ} represent the paramagnetic spin–orbit and orbital–Zeeman integrals, respectively. The kinetic energy corrections for paramagnetic spin–orbit (H^{PSO-K}) and orbital–Zeeman (H^{OZ-K}) terms are also considered. The Fermi contact and the spin–dipolar operators are denoted as $H^{FC/SD}$, while the spin–Zeeman kinetic energy correction and the magnetic field-induced spin–orbit term are represented by H^{SZ-K} and H^{BSO}, respectively. The one-body relativistic effect of spin–orbit coupling is captured by $H^{SO(1)}$, while the scalar relativistic corrections Darwin and mass–velocity are represented by $H^{Dw/Mv}$. Detailed expressions for these Hamiltonians can be found in the Supplementary Information.

The relativistic corrections to the diamagnetic component of the shieldings include (i) the linear response between the NR diamagnetic-like Hamiltonian of Equation (S11) and the Mv- and Dw-correcting Hamiltonians and (ii) the average value of H^{Dia-K} given in Equation (S12). The Hamiltonian H^{Dia-K} contains several terms: the average value of the Fermi contact plus spin–dipolar contributions induced by the external magnetic field, the orbital–Zeeman corrections to the paramagnetic spin–orbit term, the kinetic correction to the diamagnetic NR shielding contribution, and a multiple of the Dirac delta function centered on the given one [26].

Furthermore, the relativistic corrections to the shielding can be divided into two groups: ligand-dependent corrections, which depend on the chemical environment, and non-ligand-dependent (NL-dependent) corrections, which are primarily influenced by the core MOs. The ligand-dependent corrections take into account the specific interactions with surrounding ligands and their effects on the shielding. On the other hand, the NL-dependent corrections are mainly governed by the behavior of the core MOs and their contributions to the shielding. These two categories collectively contribute to the overall relativistic corrections to the nuclear magnetic shieldings.

The ligand-dependent contribution encompasses σ^{OZ-K}, σ^{PSO-K}, $\sigma_p^{(Mv/Dw)}$, and $\sigma^{SO(1)}$. On the other hand, the NL-dependent contribution encompasses all diamagnetic corrections and the remaining paramagnetic corrections. The clear separation of these contributions is illustrated in Table 1.

Table 1. Comprehensive scheme of paramagnetic and diamagnetic corrections as given by the LRESC model, including ligand-dependent and non-ligand-dependent contributions.

Paramagnetic						Diamagnetic	
Ligand-Dependent				Non-Ligand-Dependent			
σ^{OZ-K}	σ^{PSO-K}	$\sigma_p^{(Mv/Dw)}$	$\sigma^{SO(1)}$	$\sigma^{(FC/SD)-BSO}$	$\sigma^{(FC/SD)-K}$	$\sigma_d^{(Mv/Dw)}$	σ^{Dia-K}

3. Materials and Methods

The molecular systems investigated in this study include PtX_n^{-2} (X = F, Cl, Br, I; n = 4, 6) and $XCl_2Te_2Y_2H_6$ (X = Cd, Hg; Y = N, P).

For the PtF_4^{-2}, PtF_6^{-2}, $PtCl_6^{-2}$, and PtI_6^{-2} geometries, geometry optimization was performed using the Dirac program package [31] with the Dirac–Hartree–Fock (DHF) Hamiltonian and the dyall.cv3z basis set [32]. The remaining geometries of the platinum-containing systems were adopted from Refs. [8,13]. In the case of $Cl_2XTe_2Y_2H_6$, the geometries were obtained using an analytic gradient at the same level of theory.

The calculations with the new model LRESC-Loc were carried out at the Hartree–Fock (HF) level using the dyall.cv3z basis set for all atoms. These calculations were performed with the Dalton program [33]. The 4c shielding calculations were obtained using the relativistic polarization propagator [34] within the random phase approximation (4c-RPA). The dyall.cv3z basis set was employed, and the unrestricted kinetic balance prescription was applied [20]. The gauge origin was positioned at the position of the heavy atom, but for the analysis of HAVHA effects, the gauge origin was placed on tellurium atom. The localization of the wave function was performed using the Pypek–Mezey methodology [28] implemented in PySCF code [35]. The LRESC response calculations and the calculation of average values with canonical coefficients were performed using the Dalton program package. Additionally, a code developed in our group was used for the response and average value calculations with localized molecular orbitals as described in Ref. [27].

For the chemical-shift calculations of the PtX_n^{-2} systems, the $PtCl_6^{-2}$ molecule was selected as the reference. This choice was motivated by the fact that $PtCl_6^{-2}$ has been widely used as a reference in numerous theoretical and experimental studies [8,13]. By using $PtCl_6^{-2}$ as the reference, we can establish a consistent framework for the comparison and interpretation of the chemical shifts of other PtX_n^{-2} molecules in relation to this well-established reference system.

4. Results and Discussion

The whole set of molecules studied in this work is depicted in Figure 1, and specific geometric parameters can be found in the Supplementary Information.
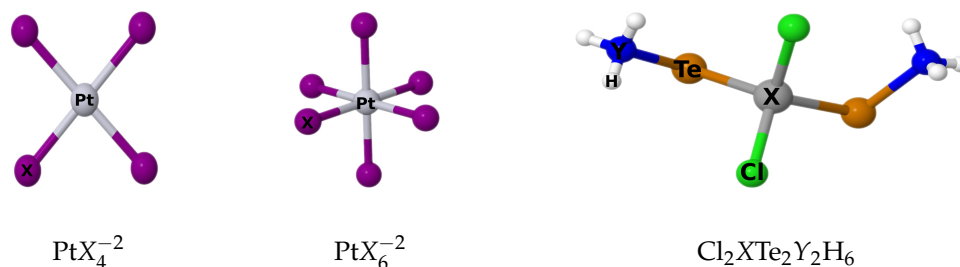
Figure 1. Representation of the molecular structures for PtX_4^{-2}, PtX_6^{-2} (X = Cl, Br, I), and $Cl_2XTe_2Y_2H_6$ (X = Cd, Hg; Y = N, P) systems.

Additionally, Table 2 provides the optimized bond lengths for Pt-F and Pt-Cl, whereas the Pt-Br and Pt-I distances were obtained from the literature.

Table 2. Bond lengths between Pt and X halogen atoms. All values are given in angstroms (Å).

	Pt–X [Å]		**Pt–X [Å]**
PtF_4^{-2}	1.90	$PtBr_4^{-2,(a)}$	2.43
PtF_6^{-2}	1.93	$PtBr_6^{-2,(b)}$	2.56
$PtCl_4^{-2,(a)}$	2.31	$PtI_4^{-2,(a)}$	2.61
$PtCl_6^{-2}$	2.36	PtI_6^{-2}	2.71

$^{(a)}$ Taken from Ref. [8]. $^{(b)}$ Taken from Ref. [13].

The orbitals associated with lone pair MOs are indicated as LP_σ and LP_π. The inner electrons of an atom are labeled as core(X), while the bonds are represented as X–Y, where X and Y are the respective atoms involved.

4.1. Platinum Complexes

In Table 3, we present the results of calculations of the isotropic nuclear magnetic shielding of the Pt atom, $\sigma(Pt)$, obtained using the LRESC and 4C-RPA methods. Both the paramagnetic and diamagnetic components are shown for comparison between the two calculation schemes. Additionally, we include the chemical shifts, $\delta(Pt)$, with respect to the $PtCl_6^{-2}$ molecule, which serves as a reference for both theoretical and experimental results.

Table 3. Nuclear magnetic shielding and chemical shift of the Pt atom in PtX_n^{-2} molecules (X = F, Cl, Br, I; n = 4, 6) calculated at LRESC and 4c-RPA levels. The values are reported in ppm.

	σ_d^{LRESC}	σ_p^{LRESC}	Total	σ_d^{4c}	σ_p^{4c}	Total	δ^{LRESC}	δ^{4c}	δ^{exp} (*)
PtF_4^{-2}	6548.0	−8400.6	−1852.6	7980.7	−6728.6	1252.1	−836.0	−4624.9	–
PtF_6^{-2}	6628.3	−18770.3	−12142.0	8062.8	−17612.8	−9550.0	9453.2	6177.1	7325
$PtCl_4^{-2}$	6644.3	−6006.9	637.4	8076.8	−6391.6	1685.2	−3326.2	−5058.1	−1626
$PtCl_6^{-2}$	6770.7	−9459.3	−2688.6	8203.3	−11576.3	−3372.9	0.0	0.0	0
$PtBr_4^{-2}$	6906.8	−5061.0	1845.8	8338.3	−5957.0	2381.3	−4534.6	−5754.2	−2676
$PtBr_6^{-2}$	7147.0	−6256.8	890.1	8585.5	−9228.6	−643.1	−3578.7	−2729.8	−1903
PtI_4^{-2}	7124.8	−2539.7	4585.0	8554.5	−3276.6	5277.9	−7273.8	−8650.8	−5522
PtI_6^{-2}	7457.3	−2117.4	5339.9	8886.3	−6079.4	2806.9	−8028.7	−6179.8	−6067

$^{(*)}$ Experimental values taken from Ref. [36] in H_2O solution, except for PtF_6^{-2} in CH_2Cl_2.

From Table 3, it can be observed that the LRESC values are not in close agreement with the 4C-RPA values. However, the overall sign of the total shielding value is consistent for the entire set of molecules, except for PtF_4^{-2} and $PtBr_6^{-2}$. It is known that the LRESC scheme encounters some difficulties in accurately reproducing magnetic shielding for nuclei in the 6th row of the periodic table, although it does capture the correct trends [21,27,37].

A more insightful analysis can be performed by considering the chemical shifts instead of the absolute values and comparing them with the experimental results. In this regard, the LRESC chemical shifts exhibit closer agreement with the experimental values compared to the 4C-RPA results. Figure 2 demonstrates that δ^{LRESC} follows the same trend as δ^{exp} across the entire set of molecules studied. However, it is important to note that these calculations were conducted under static conditions, and several effects were not taken into account.
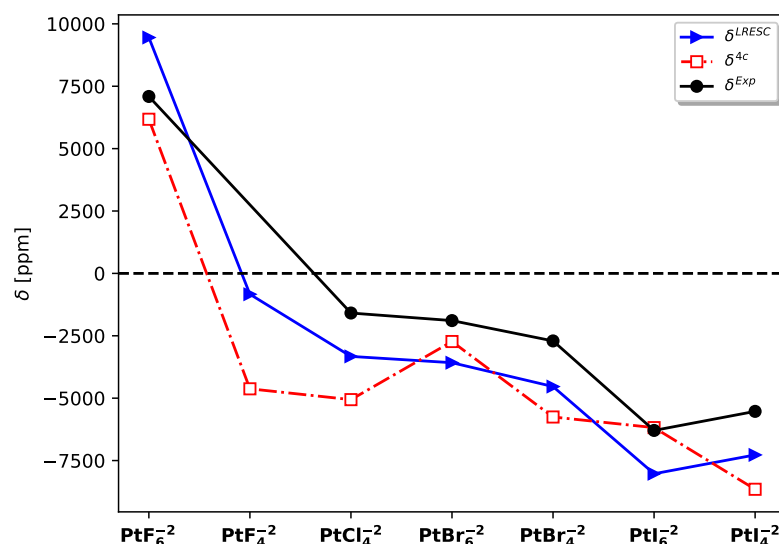

Figure 2. Chemical shift results for platinum $\delta(Pt)$ calculated at LRESC and 4c-RPA levels. Experimental values are also included. All values are given in ppm.

The primary differences between LRESC and 4C-RPA total values originate from the paramagnetic component, as the diamagnetic component exhibits a nearly constant difference. Specifically, the LRESC diamagnetic component is consistently approximately 1400 ppm lower than the corresponding 4c diamagnetic contributions. The variation of the paramagnetic component is not constant and is influenced by the ligand-dependent contributions as illustrated in Tables 4 and 5.

Table 4. Localized molecular orbital contributions to the electronic mechanisms in the LRESC formalism for the Pt atom in the PtF_4^{-2} molecule. All values are reported in ppm.

	Core(Pt)	4xCore(F)	4xPt–F	4xLP$_\sigma$F	8xLP$_\pi$F	Σ
σ_d^{NL}	−3034.7	−0.1	0.0	0.6	0.0	−3034.2
σ_d^{NR}	9379.4	39.5	51.2	34.6	77.5	9582.2
σ^{OZ-K}	533.9	0.1	0.2	0.3	−0.9	533.6
σ^{PSO-K}	597.4	0.5	282.7	34.2	−3.9	910.9
$\sigma_p^{(Mv/Dw)}$	−1633.5	−0.6	−487.7	−67.0	123.7	−2065.2
$\sigma^{SO(1)}$	1650.6	−0.4	−124.1	−15.7	−28.9	1481.6
σ^{ligand}	1148.4	−0.4	−328.9	−48.3	90.0	860.9
σ_p^{NL}	6575.9	0.0	0.0	0.0	0.0	6576.0
σ_p^{NR}	−15,771.5	−11.5	245.9	−138.6	−161.9	−15,837.5

The primary electronic mechanisms responsible for ligand-dependent relativistic effects are the well-known $\sigma^{SO(1)}$ contribution and the $\sigma_p^{(Mv/Dw)}$ contribution. Both of these mechanisms exhibit significant variations with the atomic number of the halogen atom, particularly in planar systems. The $\sigma^{SO(1)}$ contribution is widely recognized as being important in numerous atomic and molecular systems. However, the $\sigma_p^{(Mv/Dw)}$

contribution is also of comparable magnitude but with an opposite sign. As a result, the overall relativistic effects depend on the difference between these two contributions. In the case of the PtX_4^{-2} molecule, the $\sigma_p^{(Mv/Dw)}$ contribution is greater than the $\sigma^{SO(1)}$ contribution, resulting in a negative value. Moreover, this negative value becomes more pronounced (in absolute value) as the influence of the halogen substituent increases. This analysis tell us that one must include the non-SO contributions to the shieldings of heavy atoms when they are bonded to heavy atoms.

Table 5. Localized molecular orbital contributions to the electronic mechanisms in the LRESC formalism for the Pt atom in the $PtI4^{-2}$ molecule. All values are reported in ppm.

	Core(Pt)	**4xCore(I)**	**4xPt–I**	**4xLP$_\sigma$I**	**8xLP$_\pi$I**	**$\sum$**
σ_d^{NL}	−3034.2	−5.7	−0.2	0.2	0.0	−3039.9
σ_d^{NR}	9376.4	662.2	48.0	24.2	53.9	10,164.7
σ^{OZ-K}	532.4	8.7	1.5	0.5	−5.6	537.5
σ^{PSO-K}	312.9	12.3	402.8	37.5	28.4	793.8
$\sigma_p^{(Mv/Dw)}$	−2197.7	33.7	−1065.6	−35.6	−102.5	−3367.7
$\sigma^{SO(1)}$	922.0	−117.0	−146.9	35.4	453.7	1147.2
σ^{ligand}	−430.4	−62.3	−808.1	37.7	373.9	−889.1
σ_p^{NL}	6575.0	0.0	1.1	−0.2	0.0	6575.8
σ_p^{NR}	−8754.3	−332.7	714.0	117.2	200.5	−8055.3

Tables 4 and 5 provide insights into the ligand-dependent and non-ligand-dependent contributions to the nuclear magnetic shieldings of the platinum atom, focusing on the localized molecular orbitals. These contributions can be categorized into core orbitals, lone pairs, and bond orbitals. It is evident that the non-ligand-dependent corrections remain unaffected by the substituent atom, with the primary contribution originating from the platinum core orbitals. On the other hand, for the ligand-dependent contribution, the core orbitals of platinum and Pt-X bond orbitals play crucial roles in the $\sigma_p^{(Mv/Dw)}$ correction, while $\sigma^{SO(1)}$ arises from the platinum core orbitals. However, when the weight of the halogen atom increases, such a contribution is reduced and the contribution of the lone pairs becomes important, reaching the 50% of the platinum core contributions. As shown in that Tables, the main contribution to $\sigma_p^{(Mv/Dw)}(Pt)$ arises from the core(Pt) and the bonding Pt-X being X = F, Cl, Br, I. There is also a contribution from the LP_π of the atom X. When X = I, $\sigma_p^{(Mv/Dw)}(Te)$ is around 3 times the contribution of $\sigma^{SO(1)}(Pt)$. This becomes 1.5 times when X = F. The importance of HAVHA effects are clearly shown in this case.

At the NR level, the diamagnetic component of platinum $\sigma_d^{NR}(Pt)$ exhibits a similar trend for the whole set of molecules and experiences an increase of less than 600 ppm from F to I atoms. The core orbital contributions of platinum remain independent of the substituent halogen atom, constituting approximately 92% to 98% of the total σ_d^{NR}. However, the core orbitals of the substituent atom play a crucial role in determining the variation in this component, ranging from 40 ppm for F to 662 ppm for I. The combination of these contributions determines the overall behavior of σ_d^{NR}.

On the other hand, the NR paramagnetic component of platinum shielding $\sigma_p^{NR}(Pt)$ displays a significant variation depending on the substituent halogen atom, ranging from −15,838 ppm for F to −8055 ppm for I. Analysis of the molecular orbitals reveals that the core orbitals of Pt are consistently negative and dominant, ranging from −15,772 ppm for F to −8754 ppm for I. The core orbitals of the halogen atoms also contribute negatively, with a negligible contribution for F but progressively increasing with the atomic weight of the halogen, accounting for up to 4% of the platinum core orbitals contribution in the case of I.

Tables 4 and 5 further illustrate the distinct behavior of the remaining MOs. The Pt-X bond orbitals consistently contribute positively but at one or two orders of magnitude lower

than the platinum core orbitals. In contrast, the σ-type and π-type lone pair contributions exhibit similar behavior, with negative values for F substituents that transition to positive values for the other halogens. These lone-pair contributions can collectively account for up to 10% of the platinum core orbitals contribution in the case of the $PtCl_4^{-2}$ molecule.

In Figure 3, the contributions of localized molecular orbitals to the $\sigma^{SO(1)}$ and $\sigma_p^{(Mv/Dw)}$ relativistic corrections are presented for the entire set of molecules under study. Additionally, for PtX_6^{-2}, the contribution of σ^{PSO-K} is also shown. The $\sigma^{SO(1)}$ mechanism originates from the core electrons of platinum, but as the weight of the halogen increases, the lone-pair orbitals become significant and change sign from negative to positive. The primary contribution to the $\sigma_p^{(Mv/Dw)}$ mechanism also arises from the core orbitals of platinum. Furthermore, the σ^{PSO-K} mechanism exhibits a comparable magnitude to $\sigma^{SO(1)}$ in PtF_6^{-2} and $PtCl_6^{-2}$ molecules, with the core orbitals of platinum and Pt-X bonds playing a significant role.
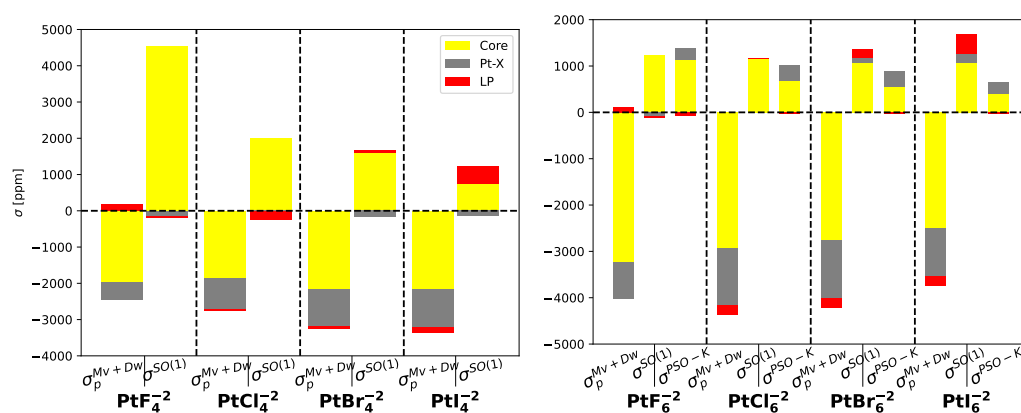

Figure 3. Contributions of core orbitals, bond orbitals, and lone-pair orbitals to the $\sigma_p^{(Mv/Dw)}$ and $\sigma^{SO(1)}$ mechanisms on Pt in PtX_4^{-2} (**left**) and PtX_6^{-2} (**right**) molecules. The σ^{PSO-K} mechanism is also displayed for PtX_6^{-2}.

We will now analyze the $\sigma(Pt)$ in PtX_6^{-2} (X = F, Cl, Br, I) molecules, as shown in Table 3. This allows us to observe the influence of the number of substituent halogen atoms as well as the influence of the change in geometry.

The core contributions to the paramagnetic and diamagnetic components are the same as those in PtX_4^{-2} molecules. These contributions arise from the core orbitals of Pt and are responsible for these effects.

The diamagnetic component, $\sigma_d^{NR}(Pt)$, in PtX_6^{-2} molecules is approximately 1% larger than in PtX_4^{-2} molecules. However, the contribution of platinum core orbitals slightly decreases with an increasing number of bonds, resulting in a slightly higher contribution from the other molecular orbitals. These orbitals contribute a larger percentage to the total values compared to PtX_4^{-2} molecules. Additionally, the core value of the halogen atoms increases by 31% when Pt is bonded to six halogen atoms. This analysis highlights the effect of the increased number of halogen substituents on the electronic mechanisms.

Regarding the paramagnetic component, Tables 6 and 7 reveal that the $\sigma^{SO(1)}$ relativistic correction is less significant than the $\sigma_p^{(Mv/Dw)}$ corrections and has an opposite sign. As a result, the ligand-dependent corrections to the paramagnetic component have negative values with the exceptions of PtF_4 and $PtCl_4$.
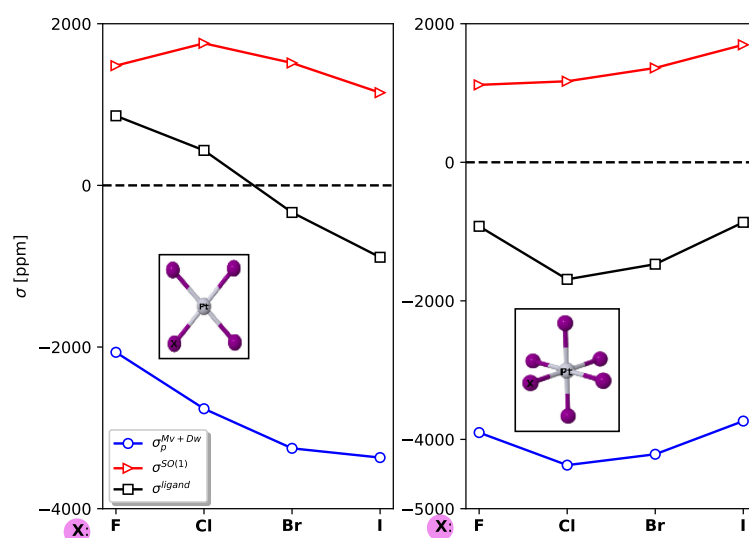
In PtX_4^{-2} molecules with D$_{4h}$ symmetry, both $\sigma^{SO(1)}$ and $\sigma_p^{(Mv/Dw)}$ corrections decrease as the weight of the substituent halogen atom increases. However, in PtX_6^{-2} molecules with O$_h$ symmetry, the behavior is opposite as illustrated in Figure 4.

Table 6. Localized molecular orbital contributions to the electronic mechanisms calculated using the LRESC formalism for the Pt atom in the PtF_6^{-2} molecule. All values are reported in ppm.

	Core(Pt)	6xCore(F)	6xPt–F	6xLP$_\sigma$F	12xLP$_\pi$F	Σ
σ_d^{NL}	−3033.1	−0.1	−1.0	0.0	0.0	−3034.2
σ_d^{NR}	9358.3	58.2	75.8	55.8	114.4	9662.5
σ^{OZ-K}	540.0	0.0	0.4	0.2	−1.9	538.7
σ^{PSO-K}	1148.1	−3.3	241.1	2.7	−67.7	1321.0
$\sigma_p^{(Mv/Dw)}$	−3226.9	−3.9	−789.9	4.6	114.6	−3901.5
$\sigma^{SO(1)}$	1242.8	−0.6	−84.4	−0.4	−39.8	1117.7
σ^{ligand}	−296.0	−7.7	−632.7	7.1	5.3	−924.0
σ_p^{NL}	6574.2	0.0	0.0	0.0	0.0	6574.2
σ_p^{NR}	−27,652.8	76.7	1589.3	−113.1	1679.5	−24,420.5

Table 7. Contributions of LMOs to the electronic mechanisms in the PtI_6^{-2} molecule as calculated using the LRESC-Loc model. All values are given in ppm.

	Core(Pt)	6xCore(I)	6xPt–I	6xLP$_\sigma$I	12xLP$_\pi$I	Σ
σ_d^{NL}	−3033.5	−8.4	−1.1	0.2	0.0	−3042.8
σ_d^{NR}	9350.2	961.6	79.9	36.7	71.7	10,500.1
σ^{OZ-K}	532.5	12.4	2.8	1.1	−9.0	539.9
σ^{PSO-K}	402.8	4.5	256.4	6.2	−37.0	632.9
$\sigma_p^{(Mv/Dw)}$	−2568.4	72.1	−1041.6	47.6	−245.0	−3735.3
$\sigma^{SO(1)}$	1146.4	−75.5	204.1	−47.5	468.6	1696.1
σ^{ligand}	−486.7	13.5	−578.3	7.5	177.6	−866.4
σ_p^{NL}	6573.8	0.0	2.4	−0.8	0.0	6575.4
σ_p^{NR}	−10,917.3	−403.5	2047.1	133.1	1314.3	−7826.3

Figure 4. Contributions of $\sigma^{SO(1)}$ and $\sigma_p^{(Mv/Dw)}$ to σ^{ligand} in PtX_4^{-2} (**left**) and PtX_6^{-2} (**right**) molecules. All values are given in ppm.

4.2. Cadmium and Mercury Complexes

Table 8 presents the paramagnetic and diamagnetic contributions to $\sigma(X)$ and $\sigma(Te)$ in the $Cl_2XTe_2Y_2H_6$ (X = Cd, Hg; Y = N, P) molecular systems, calculated using both the

LRESC and 4C-RPA methods. For the Cd atom, which belongs to the 5th row of the periodic table, the LRESC values are very close to the 4C-RPA values, with differences ranging from 0.2% to 1%. This indicates a good agreement between the two methods for Cd atom. On the other hand, for the Hg atom belonging to the 6th row of the periodic table, larger differences are observed between the LRESC and 4C-RPA values. The differences range from 16% to 18%, which is consistent with the expected behavior for an atom in the 6th row. In addition, the nuclear magnetic shielding of the Te atom is included in the table to analyze the HAVHA effect. When the total relativistic contribution cannot be explained by only including the SO mechanism, that effect is then in action. In other words, the HAVHA effects become important when the SO mechanism does not explain the trends found for the shielding of HAs that are bonded to another HA.

Table 8. Paramagnetic and diamagnetic contributions to $\sigma(X)$ and $\sigma(\text{Te})$ in the $Cl_2XTe_2Y_2H_6$ (X = Cd, Hg; Y = N, P) molecular systems, calculated using the LRESC and 4C-RPA methods. All values are given in ppm.

	Atom	σ_d^{LRESC}	σ_p^{LRESC}	Total	σ_d^{4c}	σ_p^{4c}	Total
$Cl_2CdTe_2N_2H_6$	Cd	4615.8	−167.3	4448.5	4830.1	−423.9	4406.1
	Te	4848.6	−2764.7	2083.9	5248.1	−3109.0	2039.1
$Cl_2CdTe_2P_2H_6$	Cd	4646.8	−87.1	4559.7	4861.0	−291.8	4569.2
	Te	4885.1	41.8	4927.0	5183.6	−244.9	4938.8
$Cl_2HgTe_2N_2H_6$	Hg	6953.5	4369.0	11,322.6	8526.1	4980.3	13,506.3
	Te	4948.2	−3038.5	1909.7	5246.8	−3513.7	1733.1
$Cl_2HgTe_2P_2H_6$	Hg	6989.0	4437.4	11,426.3	8559.8	5326.5	13,886.3
	Te	4985.2	−54.9	4930.3	5282.8	−318.9	4963.9

The diamagnetic component of Cd and Hg in the $Cl_2XTe_2Y_2H_6$ (X = Cd, Hg; Y = N, P) molecular systems shows quite close values when the nitrogen (N) atom is replaced by the phosphorus (P) atom, both at the LRESC and 4C-RPA levels. This similarity indicates the core nature of this component. In contrast, the paramagnetic component of Cd and Hg exhibits a small variation when the N atom is replaced by the P atom due to the two-bond coupling between X and Y. However, the influence of the surrounding environment on the total value is not significant, with values of approximately 163 ppm for Cd and 380 ppm for Hg at the 4C-RPA level. This results in a relative increase of approximately 3.7% for Cd and 2.8% for Hg when the N atom is replaced by the P atom.

As mentioned above, the influence of replacing Cd with Hg on $\sigma(\text{Te})$ provides a measure of the HAVHA effect on this parameter. Additionally, it is interesting to analyze the replacement of the atom N with the atom P. At the 4C-RPA level, the substitution of Cd by Hg in $Cl_2XTe_2N_2H_6$ molecules leads to a 15% decrease in $\sigma(\text{Te})$, while such a substitution in $Cl_2XTe_2P_2H_6$ molecules results in only a 0.5% decrease. These values demonstrate a significant HAVHA effect on $\sigma(\text{Te})$ when nitrogen is present in the molecule but a negligible effect when phosphorus is present. However, the most substantial change occurs when N is replaced by P, resulting in an increase of approximately 2900 ppm for Cd-centered molecules and 3230 ppm for Hg-centered molecules. This represents a variation of over 100% in $\sigma(\text{Te})$ from $Cl_2XTe_2N_2H_6$ to $Cl_2XTe_2P_2H_6$ molecules.

Upon analyzing the orbitals responsible for the nonrelativistic diamagnetic component (σ_d^{NR}) of transition metals Cd and Hg, it becomes evident that this component is primarily attributed to the contribution of core molecular orbitals. However, the core orbitals of Te contribute approximately 6% of the total value for Cd and 3% for Hg. On the other hand, the non-ligand-dependent contributions to the nonrelativistic paramagnetic component (σ_p^{NR}) solely originate from the core orbitals of Cd or Hg. The behavior of σ_p^{NR} and the ligand-dependent contributions to this component warrant further analysis.

In Figure 5, the contributions of the most significant ligand-dependent electronic mechanisms, namely σ^{OZ-K}, σ^{PSO-K}, $\sigma_p^{(Mv/Dw)}$, and $\sigma^{SO(1)}$, are shown for Cd, Hg, and Te in $Cl_2XTe_2Y_2H_6$ systems at the LRESC level. The ligand-dependent contributions on Cd

are relatively small compared to those on Hg in both analyzed molecules, but the behavior of each electronic mechanism is similar. Due to the comparable magnitudes of the main electronic mechanisms with opposite signs, the total ligand-dependent value is very small. Specifically, σ^{ligand}(Hg) amounts to only 66 ppm in the $Cl_2XTe_2N_2H_6$ molecule and 209 ppm in the $Cl_2XTe_2P_2H_6$ molecule. The difference arises from the change in sign of $\sigma^{SO(1)}$, which is negative in the first molecule and positive in the second.
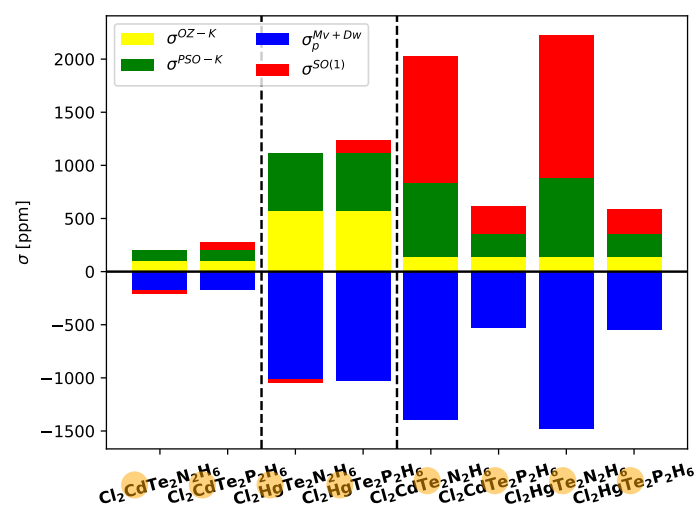

Figure 5. Ligand-dependent contributions to σ(Te), σ(Cd), and σ(Hg) in the $Cl_2XTe_2Y_2H_6$ molecular systems using localized molecular orbitals.

Figure 5 also provides a clear demonstration of the HAVHA effect on σ(Te). As mentioned earlier, the HAVHA effect is approximately 15% in $Cl_2XTe_2N_2H_6$ molecules, and the contributions of each electronic mechanism to σ^{ligand}(Te) are very similar when Cd or Hg atoms are present in the molecule. However, a significant difference arises when N is replaced by P, particularly in the reduction of $\sigma_p^{(Mv/Dw)}$, σ^{PSO-K}, and $\sigma^{SO(1)}$ (in absolute value) contributions. The molecular orbitals responsible for these changes are the *X*-Te bond orbitals, and in particular, the lone pairs of tellurium ($LP_\pi Te$) as shown in Tables provided in the electronic supporting information (ESI).

Tables 9 and 10 present the contributions of localized molecular orbitals to σ^{OZ-K}, σ^{PSO-K}, $\sigma_p^{(Mv/Dw)}$, and $\sigma^{SO(1)}$ on Cd in $Cl_2CdTe_2Y_2H_6$ (*Y* = N, P) molecules. Similarly, Tables 11 and 12 display the corresponding contributions of the Hg atom in $Cl_2HgTe_2Y_2H_6$ molecules. These tables provide detailed information about the specific molecular orbitals involved in each mechanism and their respective contributions to the overall electronic behavior of the system.

Table 9. Localized molecular orbital contributions to the electronic mechanisms of the Cd atom in the $Cl_2CdTe_2N_2H_6$ molecule as computed by the LRESC formalism. All values are provided in ppm.

	Core(Cd)	2xCore(Te)	2xCd–Te	2xCd–Cl	2xTe–N	$LP_\pi Te$	LPCl [1]	Others [2]	Σ
σ_d^{NL}	−699.4	−2.4	0.1	0.2	0.0	0.1	0.0	−0.2	−701.7
σ_d^{NR}	4799.7	288.7	17.9	20.2	10.9	22.5	42.4	115.1	5317.5
σ^{OZ-K}	102.8	3.2	−0.1	0.2	0.0	0.1	0.0	0.3	106.5
σ^{PSO-K}	2.6	3.5	38.1	38.7	0.6	4.0	11.1	0.3	98.9
$\sigma_p^{(Mv/Dw)}$	−52.7	−7.0	−32.7	−59.1	−0.4	−11.0	−12.0	−0.3	−175.2
$\sigma^{SO(1)}$	0.8	−20.5	−119.6	2.8	30.1	53.7	16.3	−0.6	−37.0
σ^{ligand}	53.5	−20.8	−114.3	−17.4	30.3	46.8	15.5	−0.3	−6.8
σ_p^{NL}	1493.4	0.0	0.3	0.1	0.0	0.2	0.1	0.0	1494.0
σ_p^{NR}	−111.7	−214.4	−463.1	−450.3	−21.7	−78.4	−203.2	−111.6	−1654.5

[1] Total $LP_\sigma Cl$ + $LP_\pi Cl$ value. [2] Total core(Cl, N) + core (N, H).

Table 10. Localized molecular orbitals contributions to the electronic mechanisms within the LRESC formalism for the Cd atom in the $Cl_2CdTe_2P_2H_6$ molecule. All values are given in ppm.

	Core(Cd)	2xCore(Te)	2xCd–Te	2xCd–Cl	2xTe–P	LP$_\pi$Te	LPCl [1]	Others [2]	$\sum$
σ_d^{NL}	−699.4	−2.4	0.1	0.3	0.0	0.1	0.0	−0.3	−701.7
σ^{NR_d}	4799.7	283.8	16.9	20.6	11.0	22.4	43.0	151.2	5348.5
σ^{OZ-K}	102.8	3.1	0.0	0.2	0.0	0.1	0.0	0.4	106.6
σ^{PSO-K}	2.5	3.4	33.7	43.1	0.6	2.3	10.8	0.3	96.8
$\sigma_p^{(Mv/Dw)}$	−53.4	−6.6	−34.6	−64.7	−0.6	−4.2	−10.9	−0.4	−175.5
$\sigma^{SO(1)}$	2.6	−18.0	−33.4	0.1	25.2	66.4	21.4	2.4	66.7
σ^{ligand}	54.5	−18.1	−34.3	−21.3	25.2	64.6	21.3	2.7	94.6
σ_p^{NL}	1493.4	0.0	0.3	0.0	0.0	0.0	0.1	0.0	1493.7
σ_p^{NR}	−112.5	−210.0	−426.0	−489.4	−20.2	−65.7	−202.9	−148.8	−1675.4

[1] Total LP$_\sigma$Cl + LP$_\pi$Cl value. [2] Total core(Cl, P) + core (P, H).

Table 11. Localized molecular orbital contributions to the electronic mechanisms based on LRESC formalism for the Hg atom in the $Cl_2HgTe_2N_2H_6$ molecule. All values are given in ppm.

	Core(Hg)	2xCore(Te)	2xHg–Te	2xHg–Cl	2xTe–N	LPTe [1]	LPCl [1]	Others [2]	$\sum$
σ_d^{NL}	−3275.2	−2.4	0.6	0.7	0.0	0.1	0.0	−0.2	−3276.4
σ^{NR_d}	9716.6	285.3	17.5	20.1	10.8	22.3	42.6	114.8	10,230.0
σ^{OZ-K}	571.7	3.2	−0.1	0.4	0.0	0.2	0.0	0.3	575.7
σ^{PSO-K}	22.3	5.0	200.2	238.6	3.1	16.3	51.2	0.2	536.8
$\sigma_p^{(Mv/Dw)}$	142.7	−6.0	−423.0	−587.4	−3.7	−81.3	−50.9	−1.3	−1011.0
$\sigma^{SO(1)}$	22.1	−27.6	−185.7	−4.3	44.5	89.4	27.4	−1.1	−35.2
σ^{ligand}	758.9	−25.5	−408.7	−352.8	43.9	24.7	27.7	−1.9	66.2
σ_p^{NL}	7105.7	0.0	0.7	−0.3	0.0	0.0	0.0	0.0	7106.1
σ_p^{NR}	−265.7	−216.2	−845.8	−913.1	−30.5	−96.5	−325.0	−110.6	−2803.3

[1] Total LP$_\sigma$Cl + LP$_\pi$Cl value. [2] Total core(Cl, N) + core (N, H).

Table 12. Contributions of localized molecular orbitals to the electronic mechanisms calculated using LRESC formalism on the Hg atom in the $Cl_2HgTe_2P_2H_6$ molecule. All values are given in ppm.

	Core(Hg)	2xCore(Te)	2xHg–Te	2xHg–Cl	2xTe–P	LPTe [1]	LPCl [1]	Others [2]	$\sum$
σ_d^{NL}	−3275.2	−2.3	0.5	0.8	0.0	0.0	0.0	−0.3	−3276.5
σ^{NR_d}	9716.6	283.9	16.7	20.3	11.1	22.5	42.8	151.5	10,265.5
σ^{OZ-K}	571.7	3.1	0.0	0.4	0.0	0.1	0.0	0.4	575.8
σ^{PSO-K}	22.2	4.5	197.6	246.8	3.3	12.6	54.0	−0.8	540.3
$\sigma_p^{(Mv/Dw)}$	130.6	−8.7	−457.3	−608.9	−4.6	−24.7	−54.7	−0.1	−1028.4
$\sigma^{SO(1)}$	0.1	−27.1	46.7	−136.8	126.9	52.8	18.6	40.2	121.4
σ^{ligand}	724.7	−28.1	−213.0	−498.5	125.5	40.8	17.9	39.8	209.0
σ_p^{NL}	7105.7	0.0	0.9	0.3	0.0	0.0	0.0	0.0	7106.9
σ_p^{NR}	−266.4	−214.8	−840.7	−936.8	−30.8	−107.4	−334.0	−147.7	−2878.6

[1] Total LP$_\sigma$Cl + LP$_\pi$Cl value. [2] Total core(Cl, N) + core (N, H).

For the Cd atom, the σ^{OZ-K}, σ^{PSO-K}, and $\sigma_p^{(Mv/Dw)}$ relativistic electronic mechanisms show similar values in both molecules when the N atom is replaced by P. The contribution of each molecular orbital follows the same trend. However, the $\sigma^{SO(1)}$ mechanism changes its sign between the two molecules, and the Cd–Te bond orbitals are responsible for the change in the final value. A similar behavior is observed for the Hg atom, where the major change occurs when N is replaced by P in the $\sigma^{SO(1)}$ mechanism, attributed to the Hg–Te

bond orbitals. The contributions change from -186 ppm in $Cl_2HgTe_2N_2H_6$ to 47 ppm in $Cl_2HgTe_2P_2H_6$, even including the negative increase due to the Hg–Cl bondings.

As mentioned earlier, the replacement of the *p*-orbital element produces significant changes in some relativistic electronic mechanisms and, consequently, in the total magnetic shielding value. This effect is more significant than the variation in the weight of the transition metal atom in this kind of molecule.

5. Conclusions

In this study, we investigated the nuclear magnetic shielding of heavy transition metals, including cadmium, platinum, and mercury, in PtX_n^{-2} (X = F, Cl, Br, I; n = 4, 6) and $Cl_2XTe_2Y_2H_6$ (X = Cd, Hg; Y = N, P) molecular systems using 4C-RPA and LRESC computational methods. We employed the LRESC-Loc formalism, which enables the analysis of different electronic mechanisms responsible for relativistic effects on heavy atoms based on localized molecular orbitals. These orbitals are classified into core orbitals, lone pairs, and bond orbitals.

The calculated chemical shifts (δ^{LRESC}) of PtX_n^{-2} molecules at the LRESC level exhibit a similar trend to the experimental values (δ^{exp}). This provides valuable insights into the molecular orbitals involved in the contributions from various corrections when the weight and number of halogen atoms vary.

Among the ligand-dependent relativistic effects, the prominent electronic mechanisms are the well-known $\sigma^{SO(1)}$ contribution and $\sigma_p^{(Mv/Dw)}$, which have opposite signs. In planar PtX_4^{-2} systems with D_{4h} symmetry, both $\sigma_p^{(Mv/Dw)}$ and $\sigma^{SO(1)}$ decrease as the substituent halogen atom becomes heavier. However, in octahedral PtX_6^{-2} systems with O_h symmetry, the behavior is opposite. The core orbitals of platinum and Pt-X bond orbitals play crucial roles in the $\sigma_p^{(Mv/Dw)}$ correction, while $\sigma^{SO(1)}$ originates from the core orbitals of platinum.

In the case of $XCl_2Te_2Y_2H_6$ molecules, the variation in $\sigma(X)$ is relatively small, ranging from 2.8 to 3.8% when a *p*-orbital element is changed. However, when examining $\sigma(Te)$, the HAVHA effect resulting from the replacement of Cd with Hg is observed to be only between 0.5 and 15%. Nonetheless, when considering a fixed metal atom (Cd or Hg), there is a remarkable enhancement of more than 100% in $\sigma(Te)$ from $Cl_2XTe_2N_2H_6$ to $Cl_2XTe_2P_2H6$ molecules. These changes can be attributed to the molecular orbitals associated with X-Te bond orbitals and also with the lone pairs of tellurium ($LP_\pi Te$).

Furthermore, for both Cd and Hg complexes, the electronic mechanisms σ^{ligand} exhibit similar values when the N atom is replaced by P. The only difference lies in the $\sigma^{SO(1)}$ mechanism, which changes its sign between the two molecules. The variation in the final value can be attributed to the X-Te bond orbitals.

Author Contributions: Conceptualization, A.F.M. and G.A.A.; methodology, A.F.M., A.D.Z.-E. and G.A.A.; software, A.D.Z.-E.; validation, A.F.M. and A.D.Z.-E.; formal analysis, A.F.M., A.D.Z.-E. and G.A.A.; resources, J.L.M.-C., A.F.M. and A.D.Z.-E.; data curation, A.D.Z.-E.; writing—original draft preparation, A.F.M.; writing—review and editing, A.F.M., A.D.Z.-E., J.L.M.-C. and G.A.A.; supervision, A.F.M., J.L.M.-C. and G.A.A.; funding acquisition, J.L.M.-C. and G.A.A. All authors have read and agreed to the published version of the manuscript.

Data Availability Statement: The data that support the findings of this study are available within the article and its Supplementary Material.

Enabled Research at Michigan State University and the high-performance computing cluster of the IMIT institute.

References

1. Huang, C.Y.; Doyle, A.G. The Chemistry of Transition Metals with Three-Membered Ring Heterocycles. *Chem. Rev.* **2014**, *114*, 8153–8198. [CrossRef]
2. Kaupp, M.; Malkin, V.G.; Malkina, O.L. *Encyclopedia of Computational Chemistry*; Wiley: Chichester, UK, 1998; pp. 1857–1866.
3. Bühl, M.; Kaupp, M.; Malkina, O.L.; Malkin, V.G. The DFT route to NMR chemical shifts. *J. Comput. Chem.* **1999**, *20*, 91–105. [CrossRef]
4. Autschbach, J.; Ziegler, T. *Encyclopedia of Nuclear Magnetic Resonance*; Wiley: Chichester, UK, 2002; pp. 303–323.
5. Autschbach, J.; Ziegler, T. *Calculation of NMR and EPR Parameters. Theory and Applications*; Wiley-VCH: Weinheim, Germany, 2004; pp. 249–264.
6. Autschbach, J. *The Calculation of NMR Parameters in Transition Metal Complexes*; Springer: Berlin/Heidelberg, Germany, 2004; pp. 1–48.
7. Vícha, J.; Novotny, J.; Komorovsky, S.; Straka, M.; Kaupp, M.; Marek, R. Relativistic Heavy-Neighbor-Atom Effects on NMR Shifts: Concepts and Trends Across the Periodic Table. *Chem. Rev.* **2020**, *120*, 7065–7103. [CrossRef] [PubMed]
8. Gilbert, T.M.; Ziegler, T. Prediction of ^{195}Pt NMR Chemical Shifts by Density Functional Theory Computations: The Importance of Magnetic Coupling and Relativistic Effects in Explaining Trends. *J. Phys. Chem. A* **1999**, *103*, 7535–7543. [CrossRef]
9. Dean, R.R.; Green, J.C. Platinum-195 and phoshorus-31 nuclear magnetic resonance studies of some platinum hydrides. *J. Chem. Soc. A* **1968**, pp. 3047–3050. [CrossRef]
10. Preetz, W.; Peters, G.; Bubitz, D. Preparation and Spectroscopic Investigations of Mixed Octahedral Complexes and Clusters. *Chem. Rev.* **1996**, *96*, 977. [CrossRef] [PubMed]
11. Drews, H.; Preetz, W. Calculation of ^{19}F and ^{195}Pt NMR Shifts of Fluoro-Chloro-Bromo-Platinates(IV). *Z. Naturforschung* **1997**, *52*, 9435.
12. Fowe, E.P.; Belser, P.; Daul, C.; Chermette, H. Assessment of theoretical prediction of the NMR shielding tensor of ^{195}PtCl$_x$Br$_{6-x}^{2-}$ complexes by DFT calculations: Experimental and computational results. *Phys. Chem. Chem. Phys.* **2005**, *7*, 1732–1738. [CrossRef]
13. Burger, M.R.; Kramer, J.; Chermette, H.; Koch, K.R. A comparison of experimental and DFT calculations of ^{195}Pt NMR shielding trends for [PtX$_n$Y$_{6-n}$]$^{2-}$ (X, Y = Cl, Br, F and I) anions. *Magn. Reson. Chem.* **2010**, *48*, S38–S47. [CrossRef]
14. Malkin, V.G.; Malkina, O.L.; Erikson, L.A.; Salahub, D.R. *Modern Density Functional Theory: A Tool for Chemistry*; Elsevier: Amsterdam, The Netherlands, 1995.
15. Autschbach, J. Analyzing NMR shielding tensors calculated with two-component relativistic methods using spin-free localized molecular orbitals. *J. Chem. Phys.* **2008**, *128*, 164112. [CrossRef]
16. dos Reis Lino, J.B.; Sauer, S.P.A.; Ramalho, T.C. Enhancing NMR Quantum Computation by Exploring Heavy Metal Complexes as Multiqubit Systems: A Theoretical Investigation. *J. Chem. Phys. A* **2020**, *124*, 4946. [CrossRef] [PubMed]
17. Vícha, J.; Komorovsky, S.; Repisky, M.; Marek, R.; Straka, M. Relativistic Spin–Orbit Heavy Atom on the Light Atom NMR Chemical Shifts: General Trends Across the Periodic Table Explained. *J. Chem. Theory Comput.* **2018**, *14*, 3025–3039. [CrossRef] [PubMed]
18. Morishima, I.; Endo, K.; Yonezawa, T. Effect of the heavy atom on the nuclear shielding constant. I. The proton chemical shifts in hydrogen halides. *J. Chem. Phys.* **1973**, *59*, 3356–3364. [CrossRef]
19. Edlund, U.; Lejon, T.; Pyykkö, P.; Venkatachalam, T.K.; Buncel, E. 7Li, 29Si,' 1 9 S n , and 207PbNMR Studies of Phenyl-Substituted Group 4 Anions. *J. Am. Chem. Soc.* **1987**, *109*, 5982. [CrossRef]
20. Maldonado, A.F.; Aucar, G.A. The UKB prescription and the heavy atom effects on the nuclear magnetic shielding of vicinal heavy atoms. *Phys. Chem. Chem. Phys.* **2009**, *11*, 5615. [CrossRef]
21. Maldonado, A.F.; Melo, J.I.; Aucar, G.A. Theoretical analysis of NMR shieldings of group-11 metal halides on MX (M = Cu, Ag, Au; X = H, F, Cl, Br, I) molecular systems, and the appearance of quasi instabilities on AuF. *Phys. Chem. Chem. Phys.* **2015**, *17*, 25516–25524. [CrossRef]
22. Kaupp, M.; Malkina, O.L.; Malkin, V.G.; Pyykkö, P. How Do Spin ± Orbit-Induced Heavy-Atom Effects on NMR Chemical Shifts Function? Validation of a Simple Analogy to Spin ± Spin Coupling by Density Functional Theory (DFT) Calculations on Some Iodo Compounds. *Chem. Eur. J.* **1998**, *4*, 118. [CrossRef]
23. Novotný, J.; Vícha, J.; Bora, P.L.; Repisky, M.; Straka, M.; Komorovsky, S.; Marek, R. Linking the Character of the Metal–Ligand Bond to the Ligand NMR Shielding in Transition-Metal Complexes: NMR Contributions from Spin–Orbit Coupling. *J. Chem. Theory Comput.* **2017**, *13*, 3586–3601. [CrossRef]
24. Melo, J.I.; Ruiz de Azúa, M.C.; Giribet, C.G.; Aucar, G.A.; Romero, R.H. Relativistic effects on the nuclear magnetic shielding tensor. *J. Chem. Phys.* **2003**, *118*, 471–486. [CrossRef]
25. Melo, J.I.; Ruiz de Azúa, M.C.; Giribet, C.G.; Aucar, G.A.; Provasi, P.F. Relativistic effects on nuclear magnetic shielding constants in HX and CH$_3$X(X = Br,I) based on the linear response within the elimination of small component approach. *J. Chem. Phys.* **2004**, *121*, 6798–6808. [CrossRef]

26. Aucar, G.A.; Melo, J.I.; Aucar, I.A.; Maldonado, A.F. Foundations of the LRESC model for response properties and some applications. *Int. J. Quantum Chem.* **2018**, *118*, e25487. [CrossRef]
27. Zapata-Escobar, A.D.; Maldonado, A.F.; Aucar, G.A. The LRESC-Loc Model to Analyze Magnetic Shieldings with Localized Molecular Orbitals. *J. Phys. Chem. A* **2022**, *126*, 9519. [CrossRef]
28. Pipek, J.; Mezey, P.G. A fast intrinsic localization procedure applicable for *ab-initio* and semiempirical linear combination of atomic orbital wave functions. *J. Chem. Phys.* **1989**, *90*, 4916–4926. [CrossRef]
29. Weinhold, F. *Discovering Chemistry with Natural Bond Orbitals*; John Wiley & Sons: Hoboken, NJ, USA, 2012.
30. Melo, J.I.; Maldonado, A.F. Relativistic corrections to the electric field gradient given by linear response elimination of the small component formalism. *Int. J. Quantum Chem.* **2019**, *119*, e25935. [CrossRef]
31. Saue, T.; Bast, R.; Gomes, A.; Jensen, H.J.A.; Visscher, L.; Aucar, I.A.; Di Remigio, R.; Dyall, K.G.; Eliav, E.; Fasshauer, E.; et al. The DIRAC code for relativistic molecular calculations. *J. Chem. Phys.* **2020**, *152*, 204104. [CrossRef] [PubMed]
32. Dyall, K.G. Relativistic Quadruple-Zeta and Revised Triple-Zeta and Double-Zeta Basis Sets for the 4p, 5p, and 6p Elements. *Theor. Chem. Acc.* **2006**, *115*, 441–447. [CrossRef]
33. Dalton, a Molecular Electronic Structure Program, Release v2018.2. 2019. Available online: http://www.kjemi.uio.no/software/dalton/dalton.html (accessed on 21 May 2023).
34. Aucar, G.A.; Maldonado, A.F.; Montero, M.D.A.; Cruz, T.S. Theoretical developments and applications of polarization propagators. *Int. J. Quantum Chem.* **2018**, *119*, e25722. [CrossRef]
35. Sun, Q.; Berkelbach, T.C.; Blunt, N.S.; Booth, G.H.; Guo, S.; Li, Z.; Liu, J.; McClain, J.D.; Sayfutyarova, E.R.; Sharma, S.; et al. PySCF: The Python-based simulations of chemistry framework. *WIREs Comput. Mol. Sci.* **2018**, *8*, e1340. [CrossRef]
36. Mason, J. *Multinuclear NMR*; Springer: Boston, MA, USA, 1987.
37. Melo, J.I.; Maldonado, A.F.; Aucar, G.A. Relativistic effects on the shielding of SnH_2XY and PbH_2XY (X, Y = F, Cl, Br and I) heavy atom–containing molecules. *Theor. Chem. Acc.* **2011**, *129*, 483. [CrossRef]